An International Journal of Optimization and Control: Theories & Applications
ISSN: 2146-0957 eISSN: 2146-5703
Vol.16, No.2, pp.462-477 (2026)
https://doi.org/10.36922/IJOCTA025460198

RESEARCH ARTICLE

Numerical analysis of stiffness-driven passive heave control in a semisubmersible platform

Srinivasan Chandrasekaran[1*], and Ajaya Kumar Das[2]

[1]Department of Ocean Engineering, Indian Institute of Technology Madras, Chennai, Tamil Nadu, India
[2]Department of Civil Engineering, Veer Surendra Sai University of Technology (VSSUT), Burla, Odisha, India
drsekaran@iitm.ac.in, oe23d008@smail.iitm.ac.in

ARTICLE INFO

Article History:
Received: November 10, 2025
Revised: December 4, 2025
Accepted: December 10, 2025
Published online: January 8, 2026

Keywords:
Heave motion
Mass ratio
Offshore floating platform
Passive damper
Response control
Semisubmersible

AMS Classification 2010:
76M12; 76R10; 80A20; 76D05; 65N30

ABSTRACT

In recent years, semisubmersibles have increasingly replaced fixed and semi-compliant platforms in deep water deployments. Their larger deck area and superior operational stability under severe environmental loads have contributed to their widespread use. However, excessive heave motion remains a critical design concern. Passive and active control strategies have been explored to address this concern. The present study proposes a novel passive damping system suspended beneath the platform deck to suppress excessive heave motion. The results demonstrate the effectiveness of the proposed passive damper in controlling heave motion under low and moderate sea states. At high sea states, however, its performance declines because it does not adequately suppress second-order effects and coupling between degrees of freedom. The controlled response behavior may result from complex inter-degree-of-freedom coupling effects, including second-order interactions. It requires more detailed higher-order analysis, which is beyond the scope of the present study. Additionally, the proposed damper system is uniquely driven by the buoyancy forces generated during submergence, eliminating the need for external power. Thus, the control action is inherently self-induced through the platform's motion, offering a simple, energy-efficient, and reliable solution for heave mitigation.

1. Introduction

Modern civilization relies heavily on hydrocarbon-based energy resources, primarily crude oil. However, reserves in nearshore regions have been significantly depleted over time. Structural systems traditionally employed for exploration and production in shallow waters are no longer viable for deep-sea resource extraction. Fixed offshore platforms, previously suitable for such operations, have become inadequate in addressing the challenges associated with greater water depths. Consequently, there is a growing need for alternative platform configurations capable of efficient exploration and production in deep and ultra-deep offshore environments.

Semisubmersible platforms are floating structures characterized by neutral buoyancy and partial submersion. They offer several advantages, including a small waterplane area, enhanced stability, and a large deck space; however, they still encounter challenges associated with excessive heave motion.[1-3]

Experimental studies have examined the coupled dynamic response of a tension leg platform (TLP) subjected to wave–current interactions at varying heading angles. The results revealed significant coupling between wave-induced motions and hydrodynamic loads, demonstrating the influence of heading direction on platform stability and tendon tension behavior.[4] The present study investigates the heave control of a Hai

*Corresponding Author

Yang Shi You (HYSY)-981 semisubmersible using a novel passive damper. Recent studies have demonstrated the versatility and safety of deploying semisubmersible platforms in deep-sea environments through postulated failure analyses.[2,5]

To mitigate heave motion, Travanca and Hao[6] introduced a modified hull configuration incorporating trussed heave plates, while other studies proposed the addition of conventional heave plates to improve hydrodynamic performance.[7]Zhu et al.[8] verified an improved movable heave-plate design with superior performance; however, its practical implementation requires detailed hydrodynamic validation. A tuned heave-plate configuration was also reported to provide significant improvement in vertical motion reduction, though the approach is constrained to specific tuning conditions and does not consider robustness across varying wave environments. [9] The implementation of a truss pontoon geometry above the columns has additionally been shown to enhance the resonance characteristics of semisubmersibles.[10] Furthermore, the integration of buoys along mooring lines has effectively reduced both hull responses and mooring line tensions.[5]

Passive damping systems, such as tuned mass dampers (TMDs), have been successfully employed in TLPs to suppress surge motion.[11-13] Experimental investigations have validated the efficiency of multiple TMDs in motion control across different mass ratios. Zhu et al.[14]developed an optimized passive suspension system for pitch reduction using analytical–numerical coupling; however, the study primarily targets pitch motion and does not address fully coupled multi-degree-of-freedom dynamics. Qiu et al.[15]introduced a quasi-zero-stiffness vibration isolation system for semisubmersibles and demonstrated improved low-frequency response mitigation; however, the study relies on idealized stiffness characteristics and does not fully capture nonlinear hydrodynamic effects during long-term operation. Dynamic positioning systems also contribute to mitigating platform motion in horizontal and vertical directions, as confirmed by Liang et al.[16] However, this approach is limited by its dependence on precise sensing and insufficient consideration of hydrodynamic uncertainties under harsh sea states.

The two-body interaction in full submergence has been shown to improve heave-motion reduction more effectively than conventional heave plates, which do not contact the water body, as verified both experimentally and numerically in previous studies.[17,18] Recent advancements in control technology have driven interest in artificial intelligence (AI)-assisted strategies for vibration mitigation.[19] Ahmad et al.[20] proposed a hybrid regression–proportional-integral-derivative approach to improve the dynamic stability of a floating offshore platform. Both studies yielded promising results, though broader investigations across different platform types are needed to generalize the applicability of AI-integrated control schemes.

Ma et al.[21] proposed a novel rotational inertia damper (RID) to suppress heave motion in semisubmersible platforms operating in shallow-sea conditions. They demonstrated that the RID effectively dissipated vibrational energy and significantly reduced heave responses, offering an efficient alternative to conventional damping mechanisms for floating offshore structures. Several studies have reported that the RID serves as an effective alternative for heave-motion reduction, outperforming traditional heave plates under certain conditions.[22-24] An inerter-based vibration isolation system has also been examined for reducing heave motion in semisubmersible platforms, and significant performance enhancement under wave excitation was reported; however, the analysis remains limited to idealized linear conditions and does not address nonlinear hydrodynamic effects or full-scale implementation challenges.[25]

For single-point anchor reservoir platforms, heave response has been shown to depend largely on the cylinder diameter and the deck-to-cylinder aspect ratio, providing limited flexibility for parametric tuning.[26] The tuned heave plate energy-harvesting system demonstrated efficient heave control but operated effectively only within a narrow operational frequency range.[27] Liquid column dampers and tuned liquid column ball dampers have been studied under various sea states, with tuned liquid column ball dampers exhibiting superior performance for offshore wind turbine applications.[28,29] TMDs and buoyant mass dampers have also been explored for controlling undesired motions of compliant offshore structures, with optimization efforts focused on minimizing response-reduction factors.[30-32]

Recent studies have demonstrated the effectiveness of a tuned liquid multicolumn damper in mitigating the pitch motion of semisubmersible floating offshore wind turbine substructures.[33] The study demonstrated that the tuned liquid multicolumn damper system significantly reduced platform pitch responses under combined wind and wave excitations, confirming its potential

as an efficient passive control device for floating wind applications. A novel adaptive fuzzy damping controller was developed to mitigate the coupled surge–pitch motions of semisubmersible platforms.[34] The proposed control strategy effectively adjusted damping characteristics in real time, resulting in substantial reductions in motion amplitudes and improved overall platform stability under varying sea states. The optimized design of multiple TMDs for vibration control in offshore wind turbines has also been investigated.[35] Their study demonstrated that an optimally distributed multiple-TMD configuration significantly enhanced vibration suppression efficiency and extended fatigue life compared to single-TMD systems under stochastic wind and wave loading conditions.

Previous research examined the active control of nonlinearly coupled responses of a TLP subjected to combined wind and wave excitations.[36] The research demonstrated that the proposed control strategy effectively mitigated platform motions and tendon-tension fluctuations, thereby enhancing the overall stability and safety of TLP systems in harsh marine environments. An H_2 active vibration-control strategy was also developed for offshore platforms subjected to wave-induced excitations.[37] The study demonstrated that the proposed control approach effectively minimized structural vibrations and improved motion stability, highlighting its potential for enhancing the dynamic performance of floating offshore systems under irregular sea states. Studies on the influence of actuator dynamics on the performance of active structural control systems for offshore wind turbines have also identified key limitations.[38,39] These studies reported that actuator dynamics significantly affect control effectiveness and system stability, emphasizing the need to account for actuator response characteristics during the controller design process.

Research on heave-motion mitigation using passive dampers in semisubmersible platforms remains limited, particularly for deep-water applications. Most existing studies have focused on semisubmersible platforms supporting offshore wind turbines rather than conventional deep-sea structures. In remote offshore regions, reliance on active or semi-active control systems is often impractical due to power-supply constraints. To address this gap, the present study introduces a novel passive damper system specifically designed for deep-water operations up to 1,500 m. The damper mechanism is activated through partial submergence, wherein buoyancy provides the initial restoring force required for activation. Structurally, the system comprises a rigid plate, vertical stiffeners, and an elastomeric mass. The vertical stiffeners, arranged in parallel and optimized for stiffness, are tuned to the operational frequencies of the selected semisubmersible platform. The conceptual design and configuration of this passive damper system have been patented by the authors (Patent Grant No. 202441058025, India).

2. Numerical analysis

The present study considered the HYSY-981 semisubmersible platform, developed by the China National Offshore Oil Corporation (CNOOC). The selected platform does not originally include the proposed passive damper system; therefore, the innovation lies in evaluating its performance with the inclusion of this damper. As illustrated in Figure 1, the platform comprises two submerged pontoons connected by four rectangular columns and is station-kept using a 12-point spread mooring arrangement. The platform is equipped with a passive damper system designed to mitigate heave motion. The damper is suspended beneath the deck, with a portion of its body submerged. It is enclosed within a protected compartment and supported by braces connected to the semisubmersible's columns, which prevent excessive displacement during operation. The damper assembly comprises an elastomeric mass element, a rigid plate, and a stiffness component consisting of vertical stiffeners. These stiffeners are arranged as a series of elements attached to a suspended rod extending from the lower deck, rather than as a single unit. They are positioned in an elliptical pattern inscribed within the square plan dimensions of the damper system, ensuring effective load transfer and structural stability. The details of the platform and mooring system are provided in Tables 1 and 2, respectively. The environmental parameters used in the analysis represent typical conditions of the South China Sea,[21] as summarized in Table 3. The sea state was characterized using the Joint North Sea Wave Project spectrum, while the wind load was estimated based on the American Petroleum Institute wind spectrum corresponding to a one1-hour mean wind speed. Furthermore, a nonlinear current profile varying with depth was assumed, extending to 203 meters below mean sea level.

The semisubmersible platform was numerically modeled using the hydrodynamic diffraction and response analysis module available in ANSYS Workbench 2025 R1 (ANSYS Inc, USA).

Table 1. Geometric properties of the semisubmersible platform

Parameter	**Magnitude**	**Unit**
Deck size	74.42 × 74.42 × 8.6	m
Column members (4 units)	17.385 × 17.385 × 21.46	m^3
Pontoon members (2 units)	114.07 × 20.12 × 8.54	m^3
Mass	47,533,450.8	kg
Water depth	1,500	m
Draft	19.0	m
Center of gravity below the mean water level	0.53	m
Radius of gyration for roll (R_x)	32.4	-
Radius of gyration for pitch (R_y)	32.1	-
Radius of gyration for yaw (R_z)	34.4	-

Table 2. Properties of the mooring lines of the semisubmersible platform

Specifications	**Magnitude**	**Unit**
Chain length	2,500	m
Mass per unit length	163.86	kg/m
Axial stiffness	0.67	MN/m
Equivalent cross-section	0.014	m^2
Equivalent diameter	0.095	m
Longitudinal drag coefficient	0.025	-

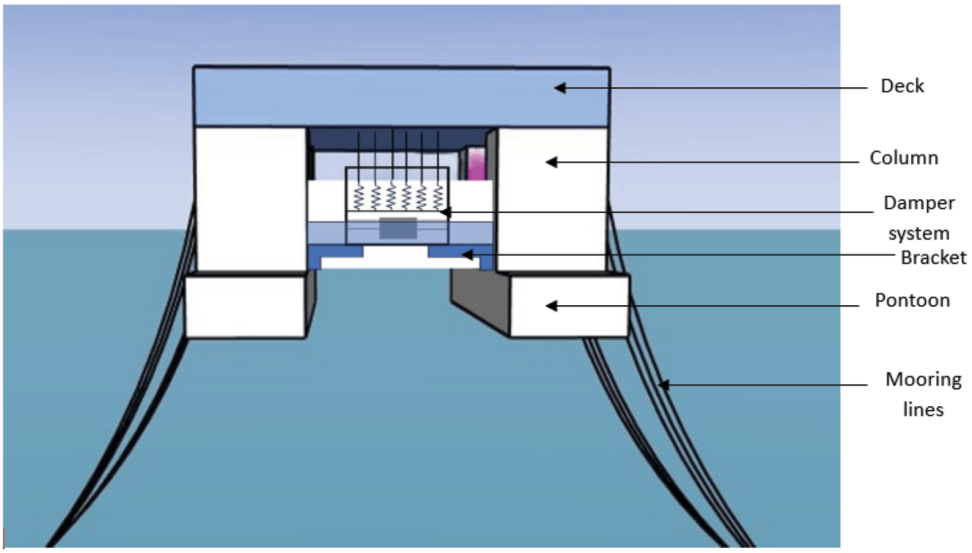

Figure 1. Schematic model of the semisubmersible platform with a passive damper

Table 3. Environmental loads

Description	**Return period**			**Unit**
	10 years Low	**50 years Moderate**	**100 years High**	
Wind speed	34.8	48.7	48.7	m/s
Significant wave height	6	11.1	13.3	m
Peak spectral period	11.2	13.6	15.5	s
Current speed	1.3	1.5	1.5	m/s

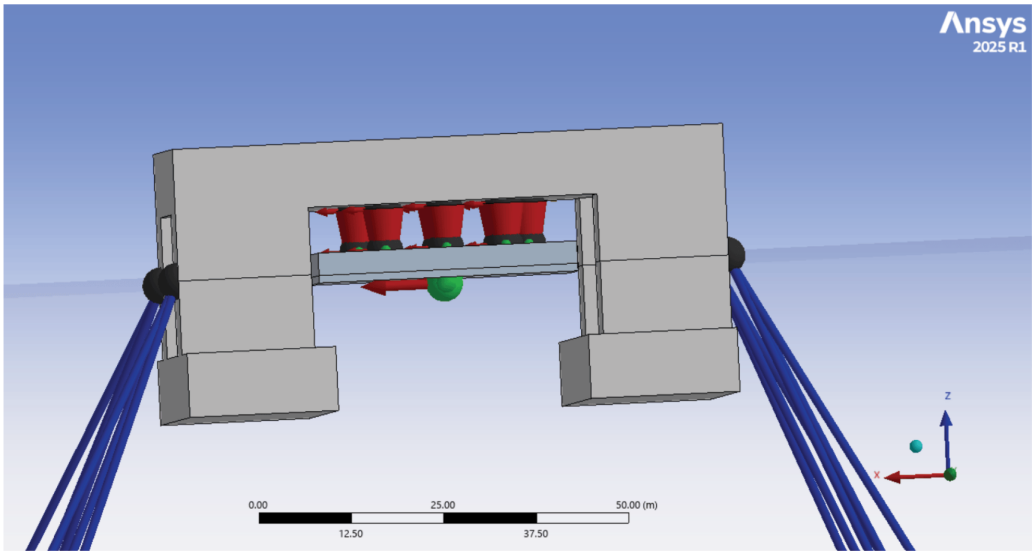

Figure 2. Numerical model of the semisubmersible platform

The model was initially created within ANSYS Workbench and subsequently transferred to the hydrodynamic analysis environment. The entire structure was modeled using a diffraction–radiation (time-domain convolution) formulation to capture hydrodynamic interactions. A finite element mesh consisting of 9,432 nodes and 9,461 elements was generated, with a maximum element size limited to 3.25 m to ensure mesh convergence.

Figure 2 presents the numerical model of the platform with the damper system. The mooring lines were modeled as catenary cable elements, extending from the fairlead connections to fixed anchors positioned 1,500 m below mean water level. A time-domain hydrodynamic response analysis was conducted for 2,000 s with a constant time step of 0.05 s, considering the combined effects of wave, wind, and current forces. The external passive damper, comprising the mass, stiffeners, and dashpots, was also modeled within the same environment. The vertical stiffeners were modeled as fender elements in the numerical simulation, enabling effective transfer of forces from the deck structure to the damper mass. Its initial design parameters were determined through a preliminary analysis conducted for representative loading conditions.

Figure 3 presents the damper configuration and corresponding free-body diagram, while Table 4 lists its physical properties. Each mooring line was assigned an axial stiffness of 0.67 MN/m and an equivalent cross-sectional area of 0.014 m^2. The analysis considered three loading conditions corresponding to low, moderate, and high sea states.

3. Results

3.1. Validation of the numerical model

To evaluate the reliability and accuracy of the proposed modeling framework, a comprehensive validation study was conducted through comparative analysis with existing literature. Specifically, the free vibration response—characterized by the absence of external force influences—was evaluated against the findings reported by Chandrasekaran and Uddin.[2] This comparison serves to verify the fidelity of the numerical model in capturing the inherent dynamic behavior of the system under undisturbed conditions. Table 4 shows the damper parameters used in the study, whereas Table 5 presents a comparison between the two studies, demonstrating that all listed parameters are consistent with previous findings.

The equation of motion is given by:

$$\begin{bmatrix} m & 0 \\ 0 & m_d \end{bmatrix} \begin{bmatrix} \ddot{x} \\ \ddot{x}_d \end{bmatrix} + \begin{bmatrix} c & 0 \\ 0 & 0 \end{bmatrix} \begin{bmatrix} \dot{x} \\ \dot{x}_d \end{bmatrix} + \begin{bmatrix} k+k_d & -k_d \\ -k_d & k_d \end{bmatrix} \begin{bmatrix} x \\ x_d \end{bmatrix} = \begin{bmatrix} F(t) \\ 0 \end{bmatrix} \tag{1}$$

where m and m_d are the mass of the platform and damper, respectively, and c is the damping coefficient of the platform. Similarly, k and k_d represent the stiffness of the semisubmersible platform and the damper, respectively. The sum of all external forces acting on the platform is grouped as $\{F(t)\}$ and assumed to act at the mass center of the platform. x, $\dot{x}$, and $\ddot{x}$ are the displacement, velocity, and acceleration of the platform, respectively, whereas x_d, $\dot{x}_d$, and $\ddot{x}_d$ are the displacement, velocity, and acceleration of the damper, respectively.

Table 4. Damper properties

Specification	Dimensions	Unit
Damper length	35	m
Damper breadth	35	m
Damper height	5	m
Mass	950,669	kg
Stiffness	4000	kN/m
Damping coefficient	0.02	-
No. of stiffeners	8	-

Table 5. Damping ratios and natural periods

Description		Present study	Reference study[2]
Natural periods	Surge	175.8 s	184.6 s
	Heave	20.9 s	21.3 s
	Pitch	28.0 s	25.4 s
Damping ratios	Surge	5%	0.2–9.5 %
	Heave	2.09 %	0.9–1.9 %
	Pitch	0.7 %	0.6–1.9 %

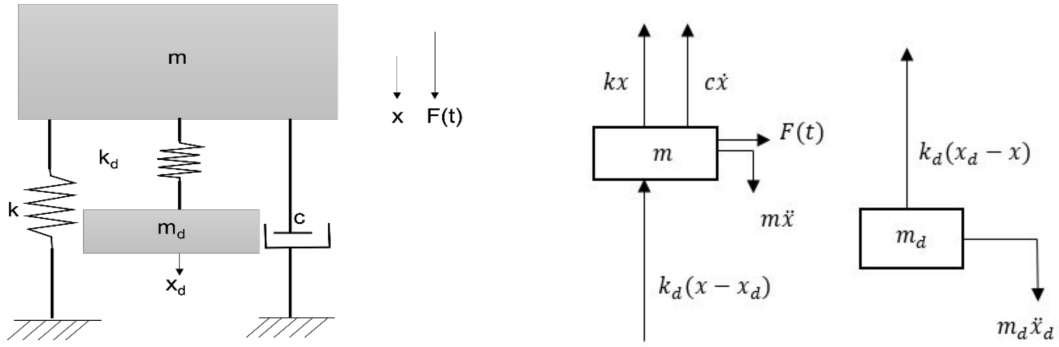

Figure 3. Damper configuration and free-body diagram

Figure 3 displays a free-body diagram of the force balance.

$$m\ \ddot{x} + c\dot{x} + kx + k_d\,(x - x_d) = F\,(t) \quad (2)$$

$$m_d\ddot{x}_d + k_d\,(x_d - x) = 0 \quad (3)$$

$$m\ \ddot{x} + c\dot{x} + kx + k_d x - k_d x_d = F\,(t) \quad (4)$$

$$m_d\ddot{x}_d + k_d x_d - k_d x = 0 \quad (5)$$

Assuming

$$x = x\ e^{-i\omega t}; \dot{x}\ = i\omega x\ e^{-i\omega t},$$

$$x_d = x_d e^{-i\omega t}; \dot{x}_d = i\omega x_d e^{-i\omega t} \quad (6)$$

As the system is tuned, it is assumed that both have the same frequency:

$$\ddot{x} = -\omega^2 x e^{-i\omega t} = -\omega^2 x \quad (7)$$

$$\ddot{x}_d = -\omega^2 x_d e^{-i\omega t} = -\omega^2 x_d \quad (8)$$

Substituting **Equation** (8) into **Equation** (5):

$$m_d(-\omega^2 x_d) + k_d x_d - k_d x = 0$$

$$x_d(k_d - m_d\omega^2) = k_d x$$

$$x_d = \frac{k_d x}{k_d - m_d\omega^2} \quad (9)$$

Substituting **Equation** (9) into **Equation** (5):

$$m\ddot{x} + c\dot{x} + kx + k_d x - k_d\left(\frac{k_d x}{k_d - m_d\omega^2}\right) = F\,(t) \quad (10)$$

Dividing both sides of **Equation** (10) by the mass m:

$$F(t) = P_0 e^{-i\omega t}$$

$$\ddot{x} + c\ \dot{x} + kx + \frac{k_d}{m}\left(x - \frac{k_d x}{k_d - m_d\omega^2}\right) = \frac{P_0 e^{-i\omega t}}{m} \quad (11)$$

Simplifying further:

$$\ddot{x} + \frac{c}{m}\dot{x} + \frac{k}{m}x + \frac{k_d}{m}\left(\frac{-m_d\omega^2}{k_d - m_d\omega^2}\right)x = \frac{P_0 e^{-i\omega t}}{m} \quad (12)$$

$$\frac{c}{c_c} = \zeta$$
$$\frac{c}{2m\omega_n} = \zeta$$
$$\frac{c}{m} = 2\zeta\omega_n$$
$$\frac{k}{m} = \omega_n^2$$
$$\frac{k_d}{m_d} = \omega_d^2$$

After substitution, **Equation** (12) can be rewritten as:

$$-\omega^2 x e^{-i\omega t} + 2\zeta\omega_n i\omega x e^{-i\omega t} + \omega_n^2 x e^{-i\omega t} + \frac{k_d}{m}\left(\frac{-m_d\omega^2}{k_d - m_d\omega^2}\right) x\, e^{-i\omega t} = \frac{P_0 e^{-i\omega t}}{m} \quad (13)$$

Simplifying and rearranging:

$$x = \frac{P_0}{m}\left[\frac{1}{\omega_n^2 - \omega^2 + \frac{k_d}{m}\left(\frac{-m_d\omega^2}{k_d - m_d\omega^2}\right) + 2\zeta\omega_n i\omega}\right] \quad (14)$$

Dividing the ω_n^2 in the numerator and denominator of the right-hand side of **Equation** (14):

$$x = \frac{P_0}{k}\left[\frac{1}{\frac{\omega_n^2-\omega^2}{\omega_n^2} + \frac{k_d}{k}\left(\frac{-m_d\omega^2}{k_d - m_d\omega^2}\right) + \frac{2\zeta i\omega}{\omega_n}}\right] \quad (15)$$

The following are the non-dimensional characteristic parameters:

(i) Mass ratio: $\mu = \frac{m_d}{m}$
(ii) Frequency ratio: $f = \frac{\omega_d}{\omega_n}$; $\beta^* = \frac{\omega}{\omega_n}$

Simplifying **Equation** (15) becomes:

$$x = \frac{P_0}{k}\left[\frac{1}{1 - \beta^{*2} + \frac{\mu f^2\beta^{*2}}{\beta^{*2} - f^2} + 2\zeta i\beta^*}\right] \quad (16)$$

To eliminate the imaginary component from the denominator, the term $1 - \beta^{*2} + \frac{\mu f^2\beta^{*2}}{\beta^{*2}-f^2} - 2\zeta i\beta^*$ is rationalized by multiplying the expression by its complex conjugate:

$$x = \frac{P_0}{k}\left[\frac{1 - \beta^{*2} + \frac{\mu f^2\beta^{*2}}{\beta^{*2}-f^2} - 2\zeta i\beta^*}{\left(1 - \beta^{*2} + \frac{\mu f^2\beta^{*2}}{\beta^{*2}-f^2}\right)^2 + 4\zeta^2\beta^{*2}}\right] \quad (17)$$

The steady-state response, derived from **Equation** (17), is represented on an Argand diagram in the complex plane (**Figure 4**). This displacement can be expressed as:

$$x(t) = \rho sin(\overline{\omega}t - \theta) \quad (18)$$

$$\rho = \frac{P_0}{k}\left[\left(1 - \beta^{*2} + \frac{\mu f^2\beta^{*2}}{\beta^{*2} - f^2}\right)^{\mathbf{2}} + 4\zeta^{\mathbf{2}}\beta^{*\mathbf{2}}\right]^{\frac{-1}{2}} \quad (19)$$

$$\theta = \tan^{-1}\left[\frac{2\zeta g}{\left(1 - \beta^{*2} + \frac{\mu f^2\beta^{*2}}{\beta^{*2}-f^2}\right)^{\mathbf{2}} + 4\zeta^{\mathbf{2}}\beta^{*\mathbf{2}}}\right] \quad (20)$$

The dynamic magnification factor is defined as the ratio of the amplitude of the steady-state harmonic response to the static displacement produced by the same force:

$$D = \frac{\rho}{\frac{P_0}{k}} = \left[\left(1 - \beta^{*2} + \frac{\mu f^2\beta^{*2}}{\beta^{*2} - f^2}\right)^{\mathbf{2}} + 4\zeta^{\mathbf{2}}\beta^{*\mathbf{2}}\right]^{\frac{-1}{2}} \quad (21)$$

$$D = \left[\frac{\left(\beta^{*2} - f^2\right)^2}{\left(1 - \beta^{*2}\right)\left(\beta^{*2} - f^2\right) + \mu f^2\beta^{*2}\}^2 + 4\zeta^{\mathbf{2}}\beta^{*\mathbf{2}}\left(\beta^{*2} - f^2\right)^2}\right]^{\frac{1}{2}} \quad (22)$$

The amplitude of the steady-state response is influenced by several parameters, including the mass ratio (μ), frequency ratios (f, β^*), and damping ratio (ζ). To identify the optimal mass ratio (μ) corresponding to a damping ratio (ζ) of 2%, as obtained from the dynamic analysis, a numerical investigation was conducted. The average heave excitation force derived from the numerical simulation was used as the input in MATLAB, where the steady-state response of the system was evaluated using **Equation** (21) for different values of mass ratio (μ).

3.2. Response of the analytical model

The dynamic amplitude factor (DAF) of the platform's steady-state response under the action of the damper is expressed as follows[40]

$$\mathrm{DMF} = \frac{\max x(t)}{P_0/k} \quad (23)$$

Thus, it is necessary to define the upper and lower limits of the frequency ratio, which is used in **Equation** (22):

$$f = \frac{\omega_d}{\omega_n} \quad (24)$$

By tuning this frequency ratio, the maximum DAF can be calculated as:

$$\mathrm{DMF}_{\max} = \frac{\max\left(x(t)\,|_{f_1}^{f_2}\right)}{P_0/k} \quad (25)$$

where f_1 and f_2 are the lower and upper limits of the frequency ratios. Thus, the maximum response amplitudes are functions of μ, ζ, and f for given values of structural damping (ζ).

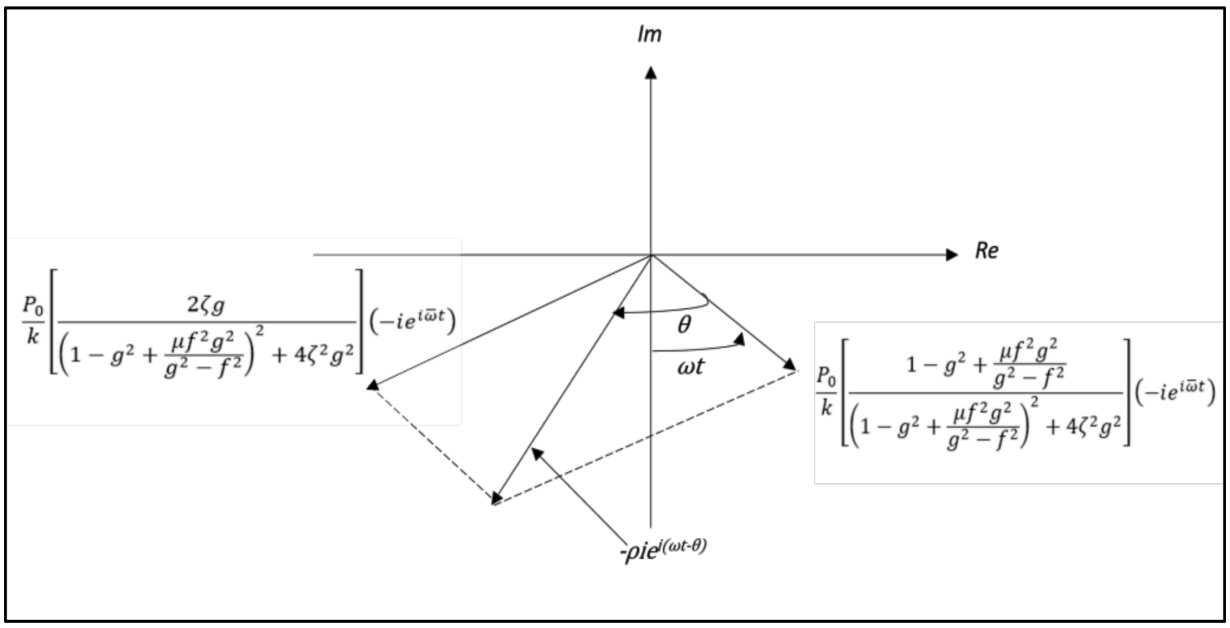

Figure 4. Steady-state response of the damper system

Table 6. Properties of the controlled mode of the platform

Specification	Dimensions	Unit
Mass of the platform	47,533,450.8	kg
Natural frequency of the platform	0.307	rad/s
Damping ratio of the platform	0.0209	-

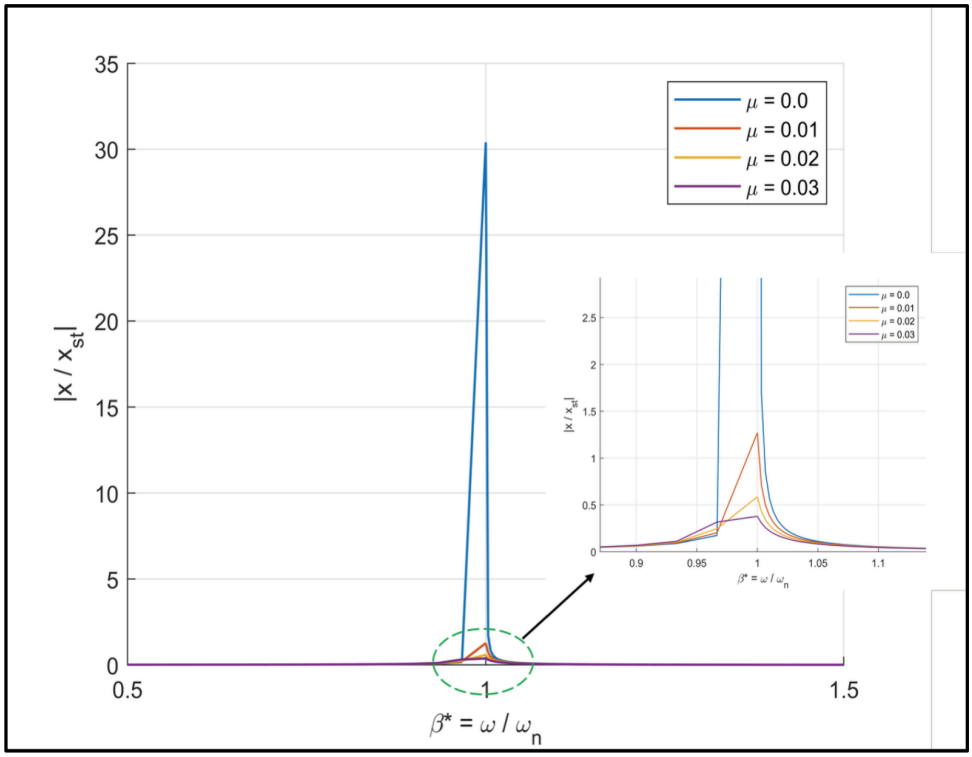

Figure 5. Dynamic amplification for different mass ratios

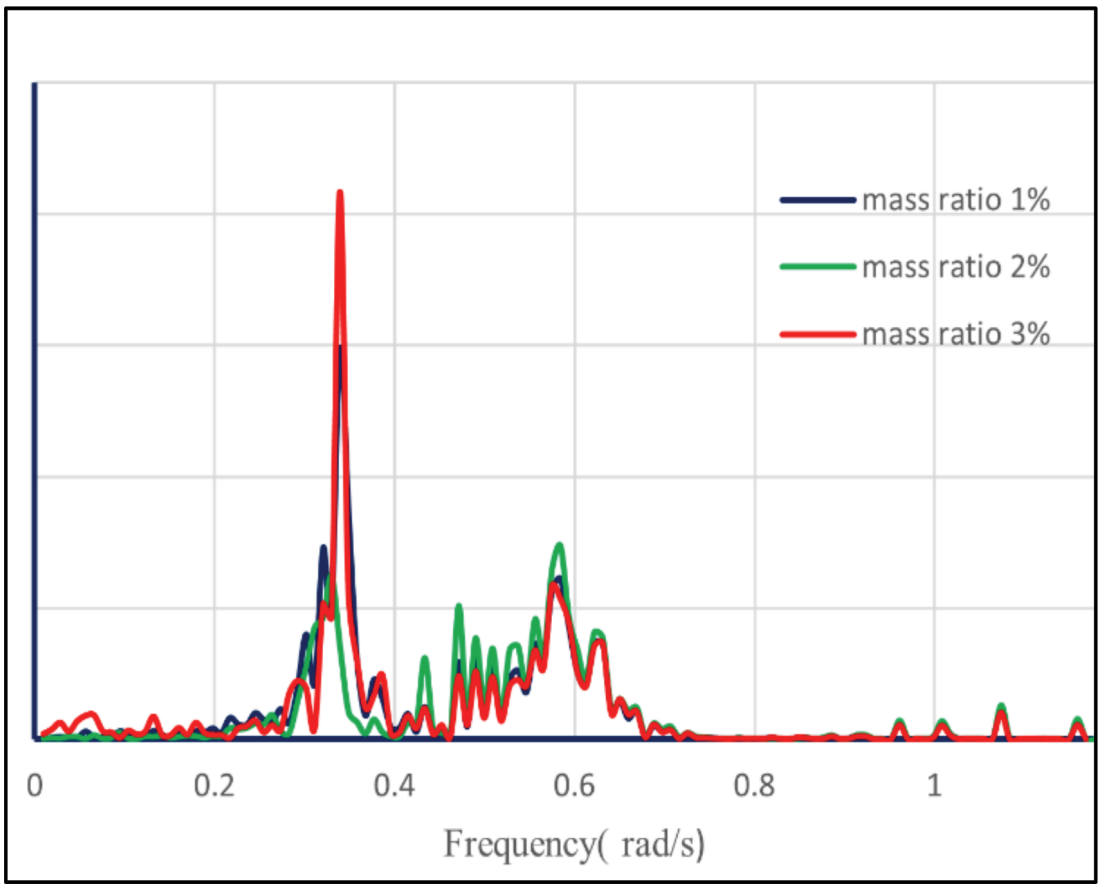

Figure 6. Heave power spectral density for different mass ratios

3.3. Parametric optimization

This section discusses the effects of frequency ranges, mass ratios, and damping ratios on the performance of the damper system. In the numerical simulation, the main parameters of a vibration mode of the semisubmersible platform were used to investigate the vibrational energy dissipation capacity of the novel damper system. The properties of the controlled mode platform are depicted in **Table 6**. In addition, an excitation frequency range of $0.5 \leq f \leq 1.5$ was considered.

The dynamic amplification for different mass ratios is shown in **Figure 5**. These responses were captured for a controlled damping ratio of 2%. The findings revealed that increasing the mass ratio reduces the response amplitude in the resonance band. However, the mass ratio is limited to 3%, as higher values are not practically feasible.[10] Nonetheless, this limitation does not clearly indicate the most effective mass ratio for the proposed damper system. Therefore, the heave power spectral density curves for the low sea state were assessed and are presented in **Figure 6**. Among the selected mass ratios, the 2% configuration demonstrated optimal performance with lower energy content. Notably, in the near-resonance region, the heave motion was reduced by nearly four times compared to the 3% mass ratio. Although the 1% mass ratio offers the advantage of a lighter damper system, it exhibited pronounced resonance peaks, which may become critical under varying sea states. Therefore, the 2% mass ratio was identified as the optimal value for damper design.

Regarding other parameters, such as frequency ratios, their influence was found to be significant in determining damper performance. Since the proposed damper relies on stiffness components—particularly vertical stiffeners—that contribute to the damping effect, the optimal stiffness (ω_d) was determined through iterative trials. The corresponding stiffness values were incorporated into the numerical model to evaluate the damper's effectiveness. Based on the analysis, the final optimized stiffness value was established and adopted for the novel damper design. **Figure 7** presents the heave spectral response for different stiffness values at 2% mass ratios.

The stiffness value of the damper was determined based on the frequency ratio, defined as the ratio between the platform stiffness and damper stiffness. Typically, 10–12% of the platform stiffness is adopted for damper design. In this study,

a frequency ratio (f) of 0.1 was selected, corresponding to a damper stiffness of approximately 4750 kN/m. The results indicate that stiffness values of 4000 kN/m and 5000 kN/m yield optimal performance. Beyond this range, such as at 6000 kN/m, a significant increase in energy content was observed in both resonance and peak wave regions. Conversely, a lower stiffness of 2000 kN/m exhibited reduced energy dissipation capability, leading to less stable behavior under different sea states.

Increasing stiffness also demands a higher number of vertical stiffeners, which increases spatial requirements and overall cost. Considering all these factors, a stiffness value of 4000 kN/m is identified as the optimal choice for design purposes. **Figure 7** shows the variations for a 2% mass ratio. However, such high-capacity stiffeners are not readily available in the commercial market. Therefore, eight stiffeners, each with a stiffness of 500 kN/m, were arranged in an elliptical configuration to achieve the desired equivalent stiffness and ensure effective damping in all loading directions.

After obtaining all the required parameters for the proposed damper, it was modeled in the ANSYS AQWA environment, consistent with the previously developed HYSY-981 platform model. Numerical simulations of the platform integrated with the damper were performed under various sea state conditions. To verify the consistency and effectiveness of the damper system, additional analyses were conducted for different wave heading angles of 0°, 30°, 45°, 60°, and 90° for each sea state.

4. Discussion

The heave response of the HYSY-981 semisubmersible platform, integrated with the proposed novel damper system, was systematically evaluated under a range of sea states as outlined in the preceding section. Comprehensive numerical simulations were conducted within the ANSYS AQWA environment to capture the coupled hydrodynamic behavior of the platform–damper system. The resulting time- and frequency-domain responses are presented and critically discussed in this section to elucidate the effectiveness of the proposed damping configuration.

Figure 8 presents a time history plot comparing the heave response behavior of the platform with and without the proposed damper system (controlled vs. uncontrolled cases). Under controlled conditions, particularly at low sea states, the platform exhibited reduced vertical vibrations. Additionally, the mean position of the platform was observed to settle slightly below its initial equilibrium level. This phenomenon occurs due to partial coupling between the heave and roll degrees of freedom. Nevertheless, the damper mechanism effectively stabilizes the motion with minimal displacement, thereby reducing discomfort at the deck level. To further examine the influence of inter-degree-of-freedom coupling, a statistical representation of the heave time-history responses for all considered sea states and varying wave heading angles is presented in **Table 7**.

Abbreviations: RMS: Root root mean square; SD: Standard standard deviation.

All controlled cases exhibited reductions in most statistical parameters, with the exception of a few metrics at higher sea states. The anomalous behavior observed under severe conditions is not fully explained by time-domain statistics alone. To clarify these deviations, frequency-domain analysis is essential, as it reveals dominant spectral energy, resonance peaks, and inter-degree-of-freedom coupling that may cause the observed responses.

Section 4.1 presents a comprehensive frequency-domain assessment of the results along with detailed explanations. The phase plots for each sea state, comparing platform responses with and without the integrated damper system, are illustrated in **Figure 9**. These plots provide a clear comparison of the dynamic behavior under controlled (with a damper) and uncontrolled (without a damper) conditions. **Figure 9** depicts the stability characteristics of the platform for both cases. With the damper attached, the platform exhibits a self-recentering tendency, resulting in shorter and more confined trajectories. Under low and moderate sea states, the platform motion forms nearly concentric circular paths, indicating improved stability and controlled heave behavior. However, in high sea states, although the overall displacement is reduced, the motion trajectories remain less orderly. This may be attributed to the influence of high-amplitude wave forces, which adversely affect the recentering capability of the platform, leading to enhanced coupling effects, vortex-induced motions, and the development of secondary vibration modes.

4.1. Frequency domain analysis

The heave response spectra for different sea states, comparing various wave heading angles with the uncontrolled case, are presented in **Figure 10**. For clarity, the uncontrolled case is shown only for the 0° wave heading angle, serving as a reference. The heave spectra for low sea states show the best performance among all cases.

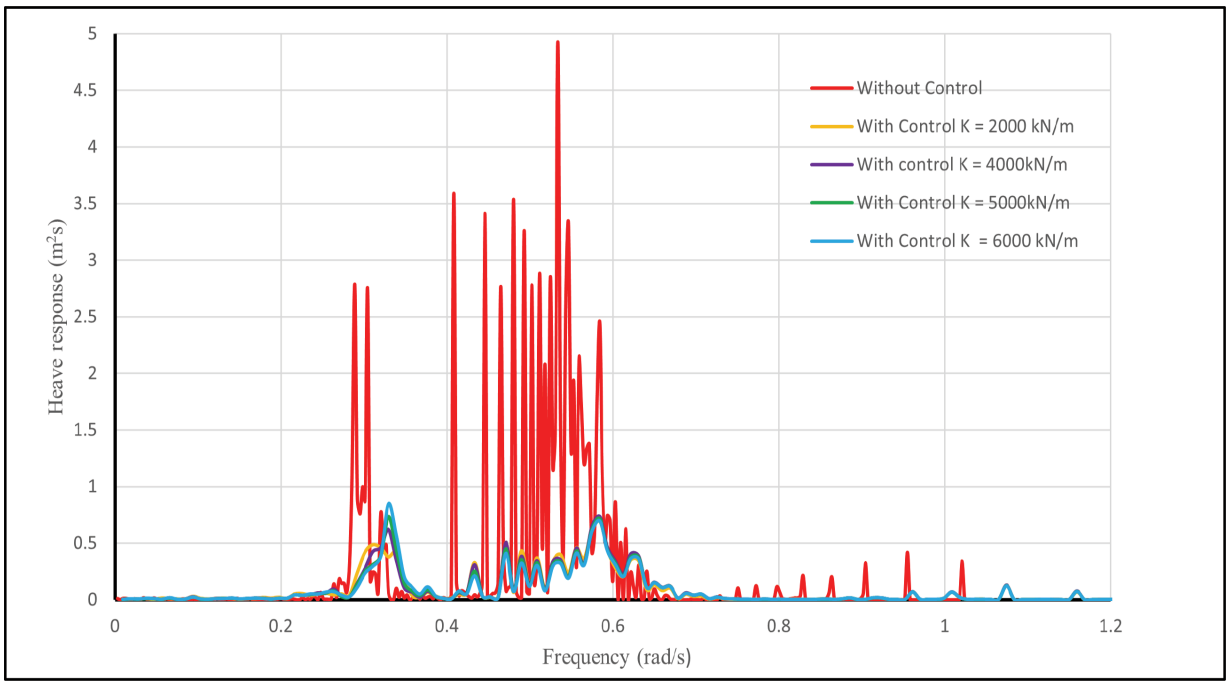

Figure 7. Heave power spectral density for different stiffness values

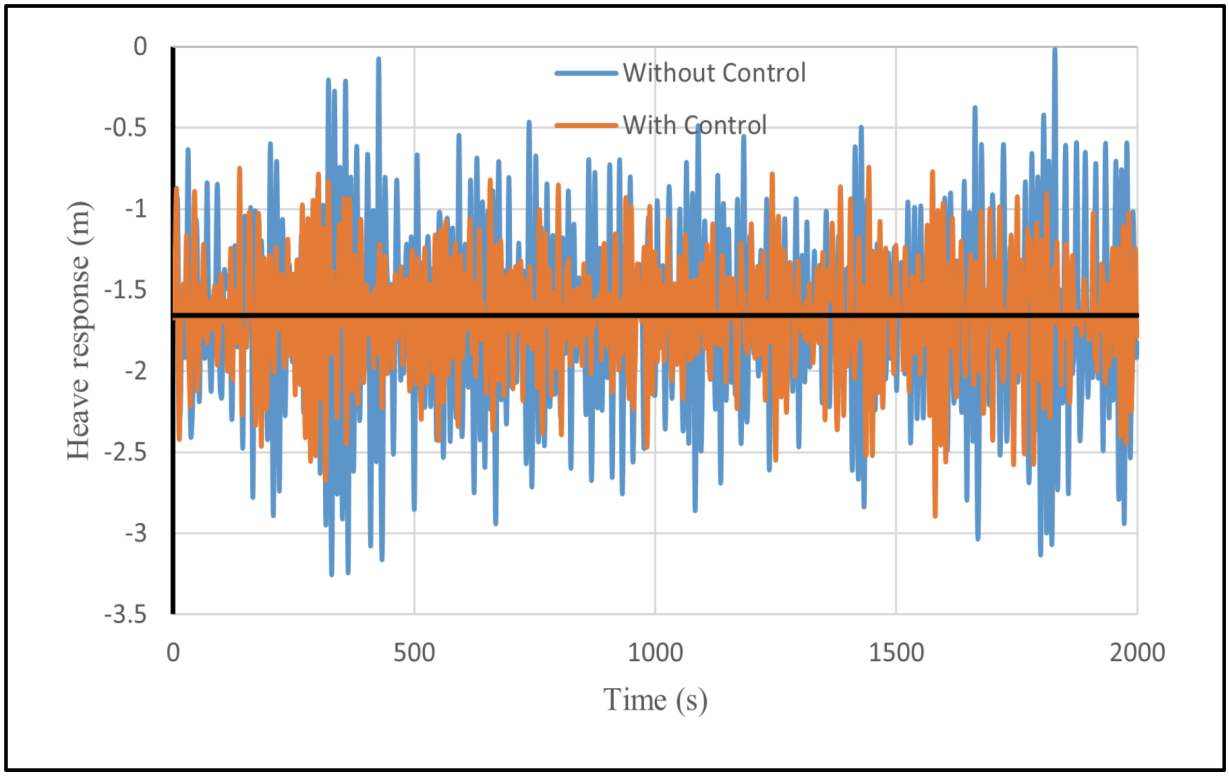

Figure 8. Heave time history

The peak spectral amplitude is reduced by nearly an order of magnitude, highlighting the effectiveness of the proposed damper system.

The damper not only significantly reduces the spectral amplitude but also smooths the response, resulting in less pronounced peaks across most wave directions. This improvement primarily occurs because the damping mechanism effectively dissipates energy induced by external excitation forces. Except for the 90° wave direction, all other headings exhibit minimal energy content in both the resonance- and wave-dominant frequency regions. Additionally, a slight frequency shift is observed across the entire range, further confirming the damper's ability to modify the system's dynamic characteristics. Overall, the results clearly demonstrate the damper's high efficiency under low sea state conditions, while maintaining its

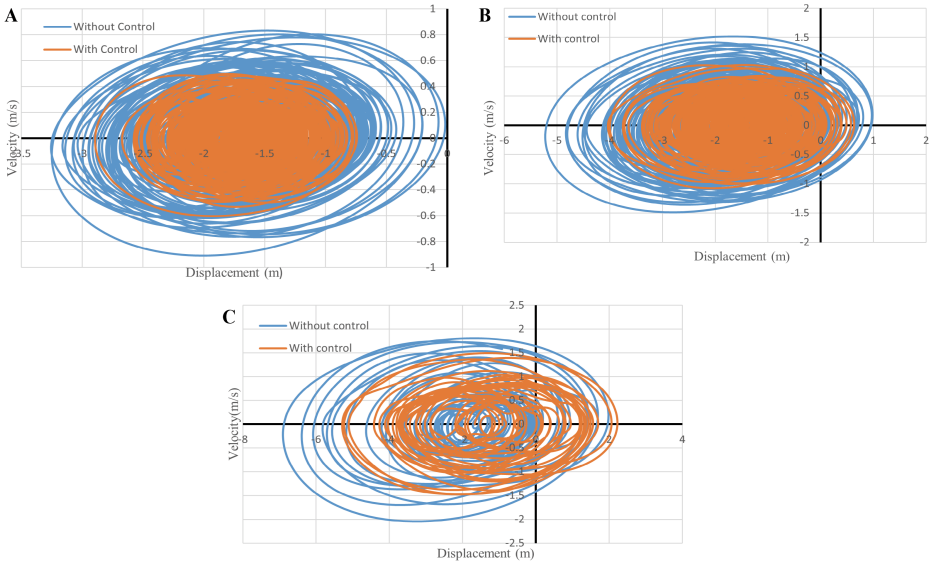

Figure 9. Heave phase plots: (A) Lowlow, (B) moderate, and (C) high sea states

Table 7. Statistical heave responses

Parameter	**Statistical heave responses**					
Direction	Without control	0°	30°	45°	60°	90°
Low sea state						
Mean (m)	−1.668	−1.656	−1.641	−1.517	−1.526	−1.527
SD (m)	0.331	0.328	0.301	0.276	0.276	0.309
RMS (m)	1.710	1.688	1.668	1.542	1.550	1.558
Max (m)	−0.017	−0.742	−0.678	−0.336	−0.385	−0.475
Min (m)	−3.255	−2.894	−2.672	−2.579	−2.469	−2.549
Moderate sea state						
Mean (m)	−1.728	−1.530	−1.507	−1.489	−1.495	−1.501
SD (m)	0.986	0.731	0.720	0.867	0.912	0.866
RMS (m)	1.989	1.696	1.670	0.771	0.783	1.733
Max (m)	0.983	0.635	0.595	0.734	0.691	0.624
Min (m)	−5.222	−4.035	−4.093	−4.080	−4.076	−4.029
High sea state						
Mean (m)	−1.761	−1.485	−1.430	−1.421	−1.431	−1.427
SD (m)	1.281	1.606	1.522	1.509	1.567	1.581
RMS (m)	2.178	1.094	0.738	1.037	1.061	1.065
Max (m)	1.970	2.223	2.008	2.153	2.494	2.195
Min (m)	−7.317	−5.287	−5.118	−5.145	−5.083	−5.242

capability to counteract external wave effects in higher sea states.

For the moderate sea state, except for the 60° and 90° wave-heading angles, all other cases exhibit significantly lower spectral peaks than in the uncontrolled condition. Although the 60° and 90° directions show relatively higher peak amplitudes, the overall energy content—represented by the area under the spectral curves—remains lower than that of the uncontrolled case. This indicates that the damper remains effective in reducing the overall heave response even under moderate sea conditions. However, the reduced performance observed around specific wave headings and frequency ranges (approximately 0.32–0.37 rad/s) may be attributed to the coupling effects between heave and pitch motions. A detailed investigation of the inter-degree-of-freedom interactions would provide deeper insight into this phenomenon, although it lies beyond the scope of the present study. Overall, the proposed damper

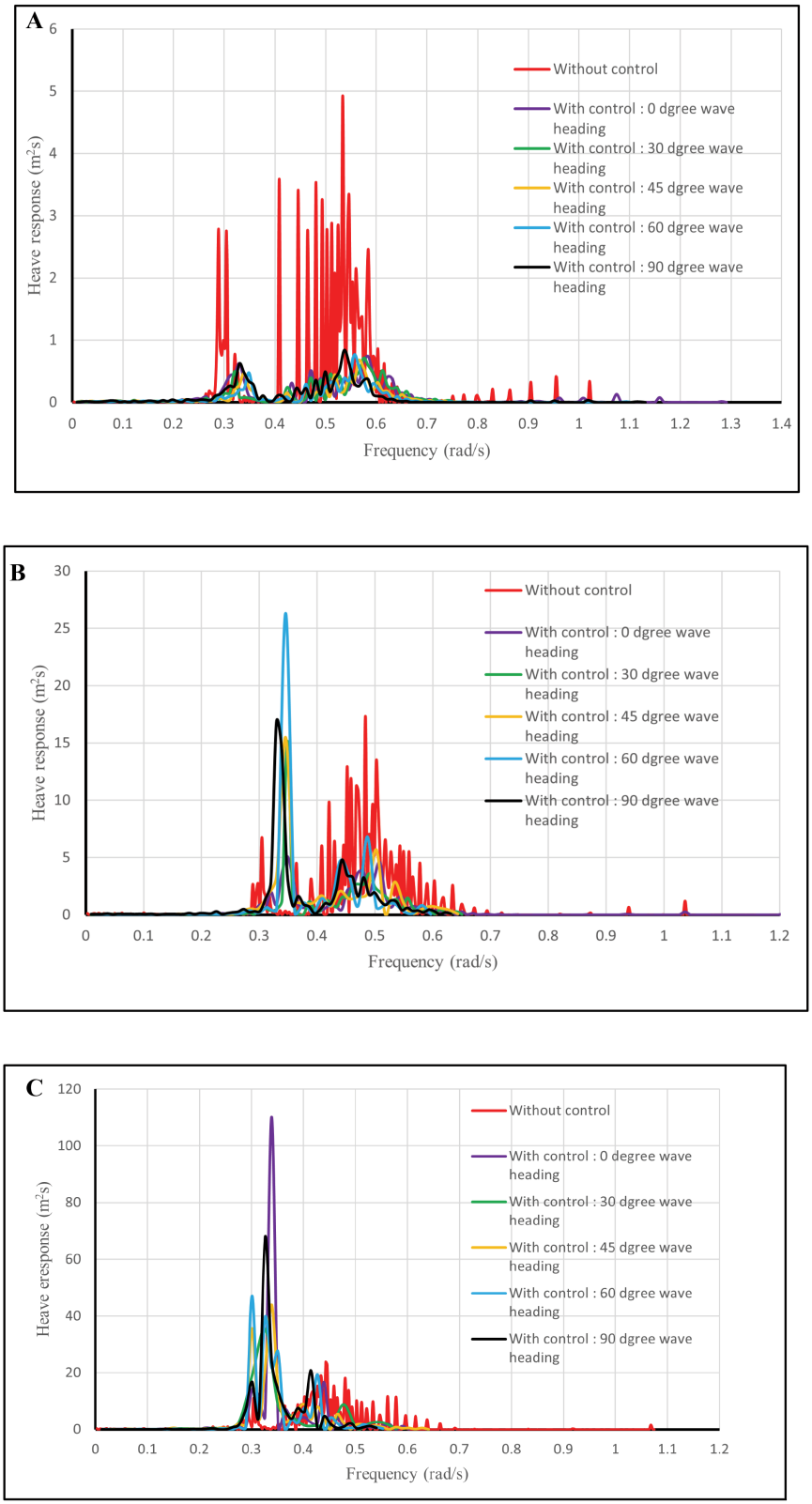

Figure 10. Heave power spectral density for different wave approach angles: (A) Lowlow, (B) moderate, and (C) high sea states

demonstrates substantial effectiveness in mitigating platform responses under moderate sea states.

The responses under high sea state conditions show comparatively reduced effectiveness of the damper system. At wave heading angles of 0°, 45°, and 90°, distinct and pronounced peaks appear near the resonance regions. This behavior can be attributed to complex interactions among the surge, roll, and pitch degrees of freedom with the heave motion. Furthermore, the presence of

second-order components becomes more prominent due to the excessive energy input from high-intensity external wave forces. It is, therefore, evident that the damper is not fully capable of counteracting the excitation forces generated under extreme sea state conditions. However, considering that such severe conditions occur infrequently in practical offshore environments, designing a damper specifically optimized for these rare events would be uneconomical. Hence, the current damper design offers an efficient and cost-effective solution for typical operational sea states while providing reasonable stability under extreme conditions.

5. Conclusion

The semisubmersible platform HYSY-981, deployed for offshore oil and gas exploration, exhibited significant heave motion that necessitates effective mitigation to ensure operational safety. In this study, passive dampers were employed to achieve the desired level of heave control, tuned over a broad frequency range. A detailed dynamic analysis was performed to evaluate heave response reduction under various sea states—low, moderate, and high. Parametric investigations were conducted for different mass ratios. In summary, the findings reveal that:

(i) The optimized mass ratio was 2 %, with a stiffness value of 4,000 kN/m.
(ii) Heave energy was reduced by 83% and 65% for low and moderate sea states, respectively.
(iii) Performance under high sea states was limited and not fully satisfactory.
(iv) Phase plot analysis demonstrates improved platform stability during damping action.

This behavior may result from complex inter-degree-of-freedom coupling effects, including second-order interactions, which require more detailed nonlinear or higher-order analysis—beyond the scope of the present study. Additionally, the proposed damper system is uniquely driven by the buoyancy forces generated during submergence, eliminating the need for external power. Thus, the control action is inherently self-induced through the platform's motion, offering a simple, energy-efficient, and reliable solution for heave mitigation.

Acknowledgments

None.

Funding

None.

Conflict of interest

The authors declare that there is no conflict of interest regarding the publication of this article.

Author contributions

Conceptualization: Srinivasan Chandrasekaran
Formal analysis: All authors
Investigation: All authors
Methodology: Ajaya Kumar Das
Software: Ajaya Kumar Das
Supervision: Srinivasan Chandrasekaran
Writing–original draft: Ajaya Kumar Das
Writing–review & editing: All authors

Availability of data

Data areis available from the corresponding author upon reasonable request.

AI tools statement

No AI tools used in this research.

References

1. Ma R, Bi K, Hao H. Mitigation of the heave response of a semi-submersible platform (SSP) using tuned heave plate inertial (THPI). *Engineering Structures.* 2018;177:357-373. https://doi.org/10.1016/j.engstruct.2018.10.013
2. Chandrasekaran S, Uddin SA. Postulated failure analyses of a spread-moored semi-submersible. *Innov Infrastruct Solut.* 2020;5(2):36. https://doi.org/10.1007/s41062-020-00309-7
3. Zhang A, Chuang Z, Liu S, Zhou L, Qu Y, Lu Y. Dynamic performance optimization of an arctic semi-submersible production system. *Ocean Eng.* 2022;244:110353. https://doi.org/10.1016/j.oceaneng.2021.110353
4. Jin R, Jiang Y, Shen W, Zhang H, Geng B. Coupled dynamic response of a tension leg platform system under waves and flow at different heading angles: An an experimental study. *Ocean Eng.* 2023;278:114563. https://doi.org/10.1016/j.oceaneng.2023.114563
5. Chandrasekaran S, Uddin SA, Wahab M. Dynamic analysis of a semi-submersible under the postulated failure of the restraining system with buoy. *Int J Steel Struct.* 2021;21(1):118-131. https://doi.org/10.1007/s13296-020-00455-y
6. Murray J, Tahar A, Yang CK. Hydrodynamics of dry tree semisubmersibles. In: *Proceedings of the ISOPE International Ocean and Polar Engineering Conference*; 2007. ISOPE-I.

7. Travanca J, Hao H. Control of wave-induced vibrations on floating production systems. *Ocean Eng.* 2017;141:35-52. https://doi.org/10.1016/j.oceaneng.2017.05.031
8. Zhu H, Ou J, Zhai G. Conceptual design of a deep draft semi-submersible platform with a moveable heave-plate. *J Ocean Univ China.* 2012;11(1):7-12. https://doi.org/10.1007/s11802-012-1871-4
9. Liang HZ-zhi, Liu K, Li LY-yu, Ou JP-ping. Dynamic performance analysis of the tuned heave plate system for semi-submersible platform. *China Ocean Eng.* 2018;32(4):422-430. https://doi.org/10.1007/s13344-018-0044-7
10. Srinivasan N, Chakrabarti S, Radha R. Response analysis of a truss-pontoon semisubmersible with heave-plates. *J Offshore Mech Arct Eng.* 2006;128(2):100-107. https://doi.org/10.1115/1.2185679
11. Chandrasekaran S, Kumar D, Ramanathan R. Dynamic response of tension leg platform with tuned mass dampers. *J Naval Archit Mar Eng.* 2013;10(2):149-156. https://doi.org/10.3329/jname.v10i2.15938
12. Suja TP, Chandrasekaran S. Response control of TLP with a single TMD under wind, wave, and current: TLP with TMD. *Mar Technol Res.* 2025;7(1). https://doi.org/10.33175/mtr 2025
13. Taflanidis AA, Angelides DC, Scruggs JT. Simulation-based robust design of mass dampers for response mitigation of tension leg platforms. *Eng Struct.* 2009;31(4):847-857. https://doi.org/10.1016/j.engstruct.2008.12.008
14. Zhu H, Hu C, Liu Y. Optimum design of a passive suspension system of a semisubmersible for pitching reduction. *J Dyn Syst Meas Control.* 2016;138(12):121003. https://doi.org/10.1115/1.4033948
15. Qiu M, Chen L, Li X. Random vibration isolation of a semi-submersible marine platform using a quasi-zero stiffness system. *Ocean Eng.* 2025;320:120334. https://doi.org/10.1016/j.oceaneng.2025.120334
16. Liang H, Li L, Ou J. Coupled control of the horizontal and vertical plane motions of a semisubmersible platform by a dynamic positioning system. *J Mar Sci Technol.* 2015;20(4):776-786. https://doi.org/10.1007/s00773-015-0322-5
17. Shin MJ, Koo WC, Kim SJ, Heo SH, Min EH. Experimental study on the reduction of vertical motion of a floating body using floating-submerged bodies. *J Soc Nav Archit Korea.* 2017;54(6):485-491. https://doi.org/10.3744/SNAK.2017.54.6.485
18. Shin MJ, Koo WC, Kim SJ. Numerical analysis of vertical motion control of a floating structure with a two-body interaction. *Int J Appl Eng Res.* 2018;13(1):511-519.
19. Perala M, Chandrasekaran S, Begovic E. Artificial intelligence-assisted station keeping for improved drillship operations. *Optim Control Theor Appl.* 2025;15(2):202-214. https://doi.org/10.11121/ijoca.2025
20. Ahmad I, M'zoughi F, Aboutalebi P, Garrido AJ, Garrido I. Advancing offshore renewable energy: integrative approaches in floating offshore wind turbine–oscillating water column systems using artificial intelligence-driven regressive modeling and proportional-integral-derivative control. *J Mar Sci Eng.* 2024;12(8):1292. https://doi.org/10.3390/jmse12081292
21. Ma R, Bi K, Hao H. A novel rotational inertia damper (RID) for heave motion suppression of a semi-submersible platform in the shallow sea. *Ocean Eng.* 2023;281:115118. https://doi.org/10.1016/j.oceaneng.2023.115118
22. Ma R, Bi K, Hao H. Wave flume tests of a semi-submersible platform controlled by a novel rotational inertia damper. *Ocean Eng.* 2021;238:109718. https://doi.org/10.1016/j.oceaneng.2021.109718
23. Ma R, Bi K, Hao H. A novel rotational inertia damper for heave motion suppression of a semisubmersible platform in the shallow sea. *Struct Control Health Monit.* 2019;26(7):e2368. https://doi.org/10.1002/stc2368
24. Ma R, Bi K, Hao H. Using an inerter-based control device to mitigate heave and pitch motions of a semi-submersible platform in the shallow sea. *Engineering Structures.* 2020;207:110248. https://doi.org/10.1016/j.engstruct.2020.110248
25. Ma R, Bi K, Hao H. Heave motion mitigation of semi-submersible platform using inerter-based vibration isolation system (IVIS). *Engineering Structures.* 2020;219:110833. https://doi.org/10.1016/j.engstruct.2020.110833
26. Tao L, Cai S. Heave motion suppression of a Spar spar with a heave plate. *Ocean Eng.* 2004;31(5-6):669-692. https://doi.org/10.1016/j.oceaneng.2003.07.001
27. Liu K, Liang H, Ou J. Numerical investigation of a tuned heave plate energy-harvesting system of a semi-submersible platform. *Energies.* 2016;9(2):82. https://doi.org/10.3390/en9020082
28. Chatterjee T, Chakraborty S. Vibration mitigation of structures subjected to random wave forces by liquid column dampers. *Ocean Eng.* 2014;87:151-161. https://doi.org/10.1016/j.oceaneng.2014.05.010
29. Nazokkar A, Dezvareh R. Vibration control of a floating offshore wind turbine using a semi-active liquid column gas damper. *Ocean Eng.* 2022;265:112574. https://doi.org/10.1016/j.oceaneng.2022.112574
30. Moharrami M, Tootkaboni M. Reducing the response of offshore platforms to wave loads using hydrodynamic buoyant mass dampers. *Eng*

Struct. 2014;81:162-174. https://doi.org/10.1016/j.engstruct.2014.09.02
31. Wang L, Bergua R, Robertson A, et al.Wright A, Zalkind D, Fowler M, Kimball R. Experimental investigation of advanced turbine control strategies and load-mitigation measures with a model-scale floating offshore wind turbine system. *Appl Energy.* 2024;355:122343. https://doi.org/10.1016/j.apenergy.2023.122343
32. Ang J, He EM, Hu YQ. Dynamic modeling and vibration suppression for an offshore wind turbine with a tuned mass damper in a floating platform. *Appl Ocean Res.* 2019;83:21-29. https://doi.org/10.1016/j.apor.2019.01.007
33. Xue MA, Dou P, Zheng J, Lin P, Yuan X. Pitch motion reduction of semisubmersible floating offshore wind turbine substructure using a tuned liquid multicolumn damper. *Ocean Eng.* 2020;218:108192. https://doi.org/10.1016/j.oceaneng.2020.108192
34. He H, Xu S, Wang L, Li B. Mitigating surge–pitch coupled motion by a novel adaptive fuzzy damping controller for a semisubmersible platform. *Ocean Eng.* 2022;258:111704. https://doi.org/10.1016/j.oceaneng.2022.111704
35. McNamara D, Pandit A, Malekjafarian A. Optimized design of multiple tuned mass dampers for vibration control of offshore wind turbines. *Ocean Eng.* 2023;278:114391. https://doi.org/10.1016/j.oceaneng.2023.114391
36. Ahmad SK, Ahmad S. Active control of nonlinearly coupled TLP response under wind and wave environments. *Ocean Eng.* 2018;170:1-12. https://doi.org/10.1016/j.oceaneng.2018.10.016
37. Li HJ, Hu SLJ, Jakubiak C. H2 active vibration control for an offshore platform subjected to wave loading. *Ocean Eng.* 2007;34(3-4):464-477. https://doi.org/10.1016/j.oceaneng.2006.03.010
38. Stewart GM, Lackner MA. The effect of actuator dynamics on active structural control of offshore wind turbines. *Eng Struct.* 2014;73:149-158. https://doi.org/10.1016/j.engstruct.2014.05.012
39. Kandasamy R, Cui F, Townsend N, et al.Foo CC, Guo J, Shenoi A, Xiong Y. A review of vibration control methods for marine offshore structures. *Ocean Eng.* 2016;127:279-297. https://doi.org/10.1016/j.oceaneng.2016.10.001
40. Gil-Martín LM, Carbonell-Márquez JF, Hernández-Montes E, Aschheim M, Pasadas-Fernández M. Dynamic magnification factors of SDOF oscillators under harmonic loading. *Appl Math Lett.* 2012;25(1):38-42. https://doi.org/10.1016/j.aml.2011.08.018

Srinivasan Chandrasekaran *is a Senior Professor (HAG) in the Department of Ocean Engineering, Indian Institute of Technology Madras, Chennai, India. He specializes in Nonlinear dynamic analysis of offshore compliant structures, earthquake-resistant analysis and design of structures, Modal pushover analysis of framed structures, base-isolated structures, Semi-active damping devices for response control of structures, Seismic analysis of offshore structures, and shell structures under shock and impact loads. He has published about 110 journal papers, authored 25 textbooks, and presented about 150 conference papers. He is an active member of many professional bodies and Societies.*
https://orcid.org/0000-0001-8346-5724

Ajaya Kumar Das *is an Assistant Professor in the Department of Civil Engineering at Veer Surendra Sai University of Technology (VSSUT), Burla, Odisha, India. His research interests include offshore structures, structural control, structural health monitoring, sustainable construction, and green concrete. He has supervised seven M.Tech students in topics related to structural control, green concrete, health monitoring, and sustainable materials. His doctoral research focuses on advanced control techniques for offshore structures. Over the past two years, he has published two research papers in international journals and three papers in international conferences.*
https://orcid.org/0009-0001-7346-2746

An International Journal of Optimization and Control: Theories & Applications
(https://accscience.com/journal/ijocta)